
**Liquid Crystals**
Publication details, including instructions for authors and subscription information:
http://www.informaworld.com/smpp/title~content=t713926090

# Comparison of bulk and thin film structures of the liquid crystal 28OBC: measurements and simulations

J. Reibel

Online publication date: 06 August 2010

**To cite this Article** Reibel, J.(1998) 'Comparison of bulk and thin film structures of the liquid crystal 28OBC: measurements and simulations', Liquid Crystals, 25: 6, 643 — 654
**To link to this Article: DOI:** 10.1080/026782998205660
**URL:** http://dx.doi.org/10.1080/026782998205660

LIQUID CRYSTALS, 1998, VOL. 25, NO. 6, 643–654

# Comparison of bulk and thin film structures of the liquid crystal 28OBC: measurements and simulations

by J. REIBEL†, M. HONIG†, U. SOHLING†, U. KOLB†, V. ENKELMANN‡ and G. DECHER†*

†Institut für Physikalische Chemie, Johannes Gutenberg-Universität Mainz, J. Welder-Weg 11, D-55099 Mainz, Germany

‡Max-Planck-Institut für Polymerforschung, Ackermannweg 10, 55021 Mainz, Germany

(*Received 8 August 1997; in final form 30 May 1998; accepted 9 June 1998*)

Freely-suspended liquid crystalline films of ethyl 4′-*n*-octyloxybiphenyl-4-carboxylate (28OBC) were prepared and transferred onto different substrates which enable detailed structural characterization. The structures of these thin film assemblies, which are only accessible in this way, were determined and compared with the crystal and molecular structure of 28OBC as formed by crystallization from toluene solution. The compound crystallizes in the monoclinic space group $P2_1/c$, $a = 11.168(1)$ Å, $b = 7.595(2)$ Å, $c = 49.106(1)$ Å, $\beta = 94.01(1)°$, $Z = 8$. The two symmetrically independent molecules of the asymmetric unit have been used as starting geometries for semi-empirical MO calculations. The difference between the experimentally observed and the optimized molecular structures is interpreted as the influence of the crystal field. The structures of the crystalline and E film phases have been investigated by SAXR and TED and the former has been found to be different from the bulk structure. The structural relationships between the different phases are discussed and a suggestion for the crystalline film structure is given as deduced from simulations of electron diffraction patterns.



## 1. Introduction

Freely-suspended (FS) films are ultrathin multilayered films with two film/air interfaces. The technique for preparing planar freely-suspended films of low molecular mass smectic liquid crystals was developed in the late 1970s [1] and since this time such films have been used to study the properties of quasi two-dimensional systems [2]. Recently FS films of liquid crystalline side group polymers have been introduced [3] and photocross-linked [4]. Due to self organization, FS films are macroscopically oriented (all molecules orient in smectic layers parallel to the film interfaces) and therefore attractive systems for structural investigations. Many of these were performed by X-ray scattering for studies of tilt and layer fluctuation profiles [5–7], as well as phase characterizations and transitions [8]. However, some in-plane structural details of ultrathin hexatic FS-films have only been accessible by investigating single film domains by transmission electron diffraction (TED) [9, 10]. Unfortunately this technique is limited by the low stability of FS films in vacuum.

A simple way to stabilize freely-suspended films is by their transfer to solid supports [11, 12]. The resulting transferred freely-suspended (TFS) films retain many of the structural and morphological features of the original FS films. In the case of ethyl 4′-*n*-octyloxybiphenyl-4-carboxylate (28OBC), TFS films have been studied intensively by optical microscopy and small angle X-ray reflection (SAXR). The phase sequence of these TFS films appeared to be similar to that of the corresponding bulk material (figure 1). Notably, their temperature stability was ~30°C higher as compared with Langmuir–Blodgett (LB) films of the same compound. A different type of defect was considered to be responsible for this observation [13]. Later, the different types of defects in both kinds of multilayer assemblies were investigated by atomic force microscopy (AFM) [14].

In continuation of our work on thin films of 28OBC, we presently report on structural investigations and comparisons of different crystalline and E phases of 28OBC in bulk and thin films. These phases are listed in the phase sequences shown in figure 1 (Cr phases and E phase).

Structural information was obtained using small angle X-ray reflection (SAXR, all phases), single crystal X-ray diffraction (SCXRD, $Cr_1$ phase) and transmission electron

* Author for correspondence. Present address: Institut Charles Sadron, 6, rue Boussingault, F-67083 Strasbourg Cedex, France.

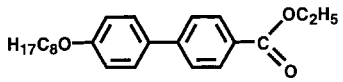


**ethyl 4'-*n*-octyloxybiphenyl-4-carboxylate (28OBC)**

**Phase sequences:**

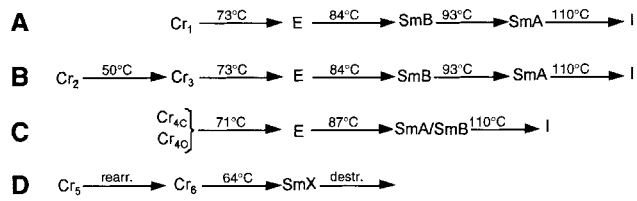


Figure 1. Structural formula of 28OBC and its phase sequences in bulk (first heating run **A**, later heating runs **B**, TFS films **C** and LB films **D**. In the assignment of the different crystalline phases of the TFS films the respective substrate is considered (i.e. $Cr_{4C}$ for a carbon substrate and $Cr_{4O}$ for an OTS coated substrate). In the case of the LB films (**D**) the transfer-induced crystalline $Cr_5$ phase rearranges at ambient temperature into the crystalline $Cr_6$ phase. When heated the film is destroyed before reaching the bulk clearing temperature. Cr = crystalline, Sm = smectic, I = isotropic.



diffraction (TED, $Cr_{4C}$ and E phases). The influence of the crystal field on the molecular geometries in the $Cr_1$ phase was deduced from semi-empirical MO calculations starting with the experimentally known molecular structures. In order to improve the structural comparison between the crystalline bulk and film phases and to investigate possible film structures, packing energies and electron diffraction patterns of various structures were calculated.

## 2. Experimental

The synthesis and the preparation of transferred freely-suspended (TFS) films of ethyl 4′-*n*-octyloxybiphenyl-4-carboxylate (28OBC), as well as the supports used for the SAXR measurements, have been described previously [13, 15, 16]. For the TED experiments carbon coated copper electron microscope grids were used as supports for the TFS films. Powder samples of 28OBC were prepared by slow solvent evaporation from toluene and ethanol solutions. Single crystals with a size in the mm range could be obtained only from the toluene solutions.

$\theta/2\theta$ X-ray powder diffractograms were obtained and small angle X-ray reflection (SAXR) measurements of the TFS films were made with a D-500 diffractometer (copper $K_\alpha$-radiation with a wavelength of $\lambda = 1.5418$ Å). The $K_\beta$ line and fluorescence were suppressed by a secondary monochromator. The reflectivity was detected by a scintillation counter and each data point represented the integrated counts of 5 seconds. The step width was 0.1° in $2\theta$. The temperature of the sample holder was measured by a Pt-100 sensor and a closed-loop temperature control regulated the temperature of the film and powder supports with an accuracy of ±1°C.

The crystal structure analysis was performed using an Enraf-Nonius CAD-4 diffractometer with $CuK_\alpha$ radiation after passing a graphite monochromator ($\lambda = 1.5405$ Å). Lattice parameters were obtained by a least squares analysis of the scattering angles of 25 reflections with $\theta > 20°$. Intensities were recorded with an $\omega/2\theta$ scan mode ($0 < \theta < 55°$). Of the 5896 reflections, 2260 unique reflections were considered observed ($I > 3\sigma(I)$). The structure was solved using direct methods (SIR) and refined by full matrix least squares analysis. The C and O atoms were assigned anisotropic temperature factors and the H atoms were refined in the riding mode with fixed isotropic temperature factors. An empirical absorption correction was applied. Final $R$ indices were $R = 0.076$ and $R_w = 0.067$ ($w = 1/\sigma^2(F)$).

Transmission electron diffraction (TED) experiments were performed using a Philips EM 300 electron transmission microscope with a tungsten hairpin cathode operating at 80 kV and a Philips EM 420 with a $LaB_6$ cathode (Denki Kagaku) operating at 100 kV. The electron beam was parallel to the normal to the planes of the TFS films. The beam had a diameter of 10–20 μm. For the determination of real space distances from the diffraction patterns, TlCl calibration diffractograms were recorded.

Molecular geometry optimization calculations were performed using semi-empirical MO calculations (MOPAC 6.0, PM 3 hamiltonian) [17].

The calculation of the packing energy and the simulations of the electron diffraction patterns were carried out using the modules CRYSTAL PACKER and DIFFRACTION 1 of the program CERIUS 3.2 [18]. The creation of unit cells for the simulation of electron diffraction patterns was performed according to the following procedure: all possible unit cells with the experimental lattice parameters ($a$, $b$ and $\gamma$) were created and the required number of planarized *trans*-like molecules were oriented in these cells with their long axes approximately parallel to the $c$-direction of the cells, considering the symmetry conditions of the respective space group. The length of the $c$-axis and the value of the angle $\beta$ in the monoclinic cells were initially set equal to the $d_{00l}$ and $\beta$ values of $Cr_1$. Close van der Waals contacts were eliminated using symmetry-allowed molecular rotations and translations and varying the monoclinic angle and the length of the $c$-axis. Generally, the reduction of the crystal packing energy required only minute changes compared with the starting parameters.

Varying intentionally the molecular orientations in the cells shows that molecular rotations of more than $\pm 3°$ or comparably small translational changes are usually not possible without increasing the packing energy remarkably.

The unit cells created in this way and possessing acceptable packing energies were used to calculate their electron diffraction patterns along the [0 0 1] zone axis. These patterns were then optimized towards the experimental diffraction pattern by slightly changing the orientation of the molecules. Changes which improved the calculated diffraction pattern with a slight increase of the packing energy were accepted and used for further optimization. While translational movements usually do not strongly affect the simulated pattern, this is very sensitive with respect to rotational changes. In most cases, rotations of only $\pm 1°$ around the $x$- or $y$-axes strongly change the density projection onto the (0 0 1) plane and correspondingly dramatically change the calculated pattern. On the other hand rotations up to 10° around the projection axis $z$ do not change the pattern remarkably.

The diffraction patterns have been calculated for diffraction angles $2\theta$ between 0° and 1.7°, $\lambda = 0.0387$ Å, setting the temperature factor equal to zero. The calculated patterns were displayed on the screen using a film scale factor of 1.1 and an intensity factor of 6.

## 3. Results and discussion

### 3.1. *Structure of the crystalline bulk phases: single crystal X-ray diffraction and molecular geometry calculations*

The LC phases of 28OBC were first investigated in the 1970s [19]. Later additional crystalline bulk phases were detected by DSC and X-ray powder diffraction ($Cr_1$, $Cr_2$ and $Cr_3$ in figure 1 [13, 15)]. Since the $Cr_2$ and the $Cr_3$ phases form only after the respective material has been heated into the LC phases and recooled, single crystals of these phases cannot be obtained. Fortunately, according to X-ray powder diffraction, the same crystalline $Cr_1$ bulk phase directly forms by crystallization from toluene or ethanol. Single crystals of the $Cr_1$ phase have been obtained from toluene and its structure was determined by single crystal X-ray structural analysis. The unit cell belongs to the monoclinic space group $P2_1/c$ with the cell parameters $a = 11.168(1)$ Å, $b = 7.595(2)$ Å, $c = 49.106(1)$ Å, $\beta = 94.01(1)°$, with $Z = 4 \times 2$ molecules per unit cell and a density $d_X = 1.133$ g cm$^{-3}$. The asymmetric unit contains two symmetrically independent molecules, whose fractional coordinates and isotropic thermal factors are given in table 1.

A projection of the single crystal unit cell is shown in figure 2. The crystal structure can be described as a layer structure with the layers parallel to the (1 0 0) plane in

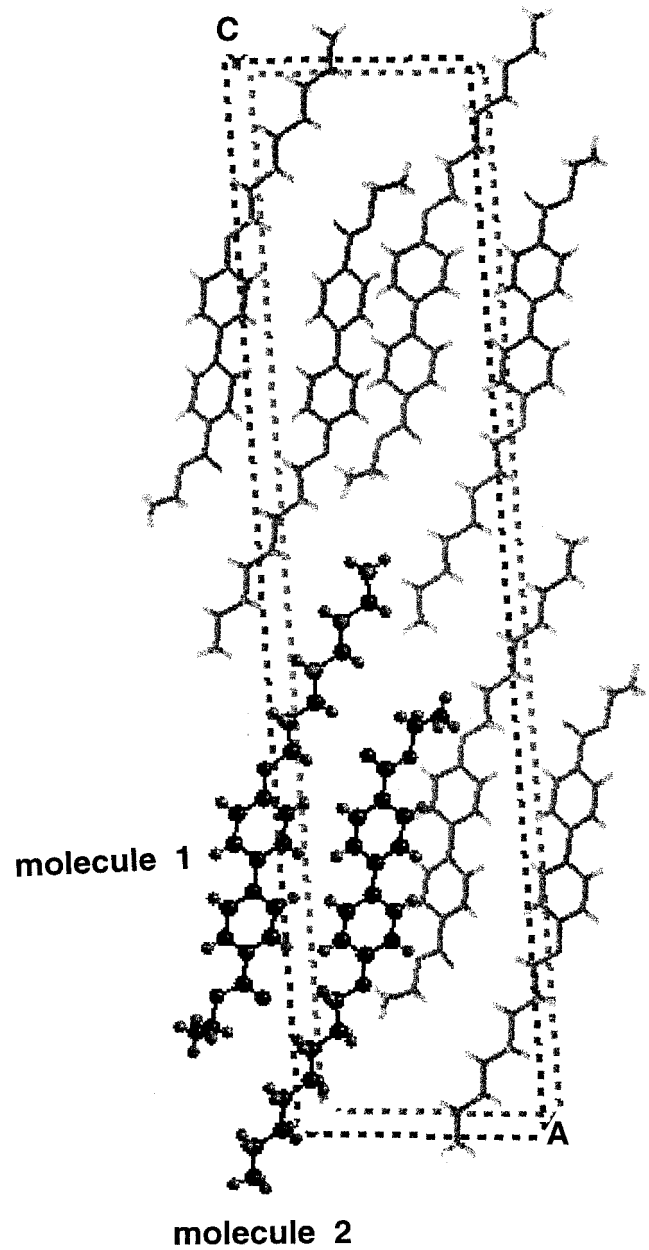


Figure 2. Projection of the unit cell of the $Cr_1$ bulk phase of 28OBC along the $b$ direction with the $a$-axis oriented horizontally and the $c$-axis oriented vertically.

which the aromatic and aliphatic parts of the molecules are arranged in an alternating fashion. The long axes of the molecules are oriented approximately in the $c$-direction with the plane of the phenyl rings parallel to the $ac$-plane. In each individual layer the octyloxy chains of neighbouring molecules point alternatingly in different directions along the $c$-axis. This allows compensation of the molecular dipole moments parallel to the long axis of the mesogenic units. A very similar crystal structure (monoclinic, space group $P2_1$, layer structure

Table 1 (*a*). Final atomic parameters: fractional coordinates and isotropic temperature factors of the $Cr_1$ phase of 28OBC. E.s.d.s are given in parentheses. Labels as shown in figures 3 (*a*) and 3 (*b*).

| Molecule 1 | | | | | | | | | |
|---|---|---|---|---|---|---|---|---|---|
| Atom | *x/a* | *y/b* | *z/c* | *U*(iso) | Atom | *x/a* | *y/b* | *z/c* | *U*(iso) |
| O1 | −0.0643(7) | 0.226(1) | 0.3400(2) | 0.0478 | C2 | 0.411(1) | 0.278(3) | 0.4887(3) | 0.1038 |
| O2 | −0.1485(9) | 0.330(1) | 0.1232(2) | 0.0785 | H21 | 0.479(1) | 0.250(3) | 0.4790(3) | 0.1690 |
| O3 | −0.3261(8) | 0.212(1) | 0.1293(2) | 0.0601 | H22 | 0.402(1) | 0.402(3) | 0.4897(3) | 0.1690 |
| C9 | −0.077(1) | 0.233(2) | 0.3120(3) | 0.0398 | C3 | 0.296(1) | 0.226(2) | 0.4734(3) | 0.0863 |
| C12 | −0.120(1) | 0.238(2) | 0.2551(2) | 0.0272 | H31 | 0.229(1) | 0.257(2) | 0.4832(3) | 0.1010 |
| C15 | −0.147(1) | 0.234(1) | 0.2253(2) | 0.0281 | H32 | 0.305(1) | 0.102(2) | 0.4731(3) | 0.1010 |
| C18 | −0.195(1) | 0.252(2) | 0.1677(2) | 0.0376 | C4 | 0.286(1) | 0.283(2) | 0.4438(3) | 0.0699 |
| C21 | −0.219(1) | 0.268(2) | 0.1377(2) | 0.0482 | H41 | 0.176(1) | 0.132(2) | 0.2124(3) | 0.0580 |
| C10 | 0.005(1) | 0.310(2) | 0.2958(2) | 0.0483 | H42 | 0.282(1) | 0.408(2) | 0.4446(3) | 0.0960 |
| H10 | 0.077(1) | 0.359(2) | 0.3040(2) | 0.0540 | C5 | 0.159(1) | 0.297(2) | 0.3994(3) | 0.0550 |
| C11 | −0.017(1) | 0.306(2) | 0.2677(3) | 0.0497 | H51 | 0.098(1) | 0.265(2) | 0.4387(3) | 0.0790 |
| H11 | 0.035(1) | 0.373(2) | 0.2572(3) | 0.0670 | H52 | 0.167(1) | 0.100(2) | 0.4296(3) | 0.0790 |
| C13 | −0.203(1) | 0.161(2) | 0.2722(2) | 0.0414 | C6 | 0.167(1) | 0.235(2) | 0.4287(2) | 0.0616 |
| H13 | −0.278(1) | 0.119(2) | 0.2645(2) | 0.0550 | H61 | 0.226(1) | 0.264(2) | 0.3891(2) | 0.0610 |
| C14 | −0.182(1) | 0.161(2) | 0.3003(3) | 0.0484 | H62 | 0.162(1) | 0.433(2) | 0.3985(2) | 0.0610 |
| H14 | −0.238(1) | 0.109(2) | 0.3116(3) | 0.0550 | C7 | 0.044(1) | 0.245(2) | 0.3833(2) | 0.0523 |
| C16 | −0.071(1) | 0.322(2) | 0.2082(3) | 0.0446 | H71 | −0.021(1) | 0.303(2) | 0.3907(2) | 0.0740 |
| H16 | 0.001(1) | 0.377(2) | 0.2154(3) | 0.0560 | H72 | 0.035(1) | 0.121(2) | 0.3852(2) | 0.0740 |
| C17 | −0.097(1) | 0.331(2) | 0.1802(3) | 0.0426 | C8 | 0.046(1) | 0.285(2) | 0.3538(2) | 0.0545 |
| H17 | −0.044(1) | 0.389(2) | 0.1689(3) | 0.0600 | H81 | 0.053(1) | 0.409(2) | 0.3517(2) | 0.1200 |
| C19 | −0.270(1) | 0.162(2) | 0.1844(2) | 0.0458 | H82 | 0.113(1) | 0.229(2) | 0.3463(2) | 0.1200 |
| H19 | −0.341(1) | 0.110(2) | 0.1762(2) | 0.0470 | C22 | −0.359(2) | 0.222(3) | 0.1000(3) | 0.0900 |
| C20 | −0.245(1) | 0.153(2) | 0.2123(3) | 0.0397 | H221 | −0.350(2) | 0.112(3) | 0.0910(3) | 0.1290 |
| H20 | −0.297(1) | 0.085(2) | 0.2227(3) | 0.0480 | H222 | −0.305(2) | 0.306(3) | 0.0932(3) | 0.1290 |
| C1 | 0.420(2) | 0.224(2) | 0.5182(3) | 0.1315 | C23 | −0.441(2) | 0.348(3) | 0.0945(3) | 0.1497 |
| H101 | 0.489(2) | 0.270(2) | 0.5280(3) | 0.1380 | H231 | −0.459(2) | 0.363(3) | 0.0755(3) | 0.1650 |
| H102 | 0.351(2) | 0.252(2) | 0.5276(3) | 0.1380 | H232 | −0.494(2) | 0.264(3) | 0.1013(3) | 0.1650 |
| H103 | 0.427(2) | 0.100(2) | 0.5168(3) | 0.1380 | H233 | −0.449(2) | 0.457(3) | 0.1036(3) | 0.1650 |



with layers parallel to the (1 0 0) plane, coplanar phenyl rings) is already known for 4-[(*S*)-2-methylbutyl]phenyl 4′-*n*-heptyloxybiphenyl-4-carboxylate [20].

The two molecules of the asymmetric unit of 28OBC have similar conformations (figure 3) but exhibit opposite orientations of the terminal octyloxy chains. Pertinent parameters characterizing their slight differences are given in table 2.

The two molecules have been used to define starting geometries for the calculation of minimized molecular geometries on the semi-empirical level. Interestingly, both starting geometries were considered rather unfavourable and have been optimized into the same final structure, figure 3 (*c*). The differences in the heat of formation between the starting and end geometries were 466.6 and 484.4 kcal $mol^{-1}$ for molecule 1 and molecule 2, respectively. In the calculated molecule all carbon and oxygen atoms lie within a common plane with the exception of the two ester oxygen atoms and the ethyl group. The latter is rotated by about 65° out of this plane. Besides slight changes in bond lengths and angles arising from the parametrization, we attribute the different out-of-plane angles to the influence of the crystal field.

### 3.2. *Structure of TFS films: electron diffraction*

Whereas the structure of films along the film normal is obtained from SAXR (films on smooth surfaces), in-plane film structures are assessed by transmission electron diffraction (TED). However, this method requires samples and substrates that are sufficiently transparent for electrons and sufficiently stable. Transferred freely-suspended films on carbon coated electron microscope grids fulfill both criteria and consequently such films of 28OBC in their $Cr_{4C}$ and E phases have been investigated by this method.

#### 3.2.1. *Electron diffraction on the $Cr_{4C}$ crystal phase*

Transmission electron diffractograms of TFS films of 28OBC in the $Cr_{4C}$ phase at ambient temperature show up to six orders of diffraction maxima in the beam geometry parallel to the layer normal. In order to determine the corresponding zone axis we use the following arguments. From earlier experiments it is known that in TFS films the smectic layers are oriented parallel to the substrate interface [12]. Therefore in films consisting of phases without molecular tilt and with the beam geometry described above, the electron beam is incident

Table 1 (*b*).

| Molecule 2 | | | | | | | | | |
|---|---|---|---|---|---|---|---|---|---|
| Atom | *x/a* | *y/b* | *z/c* | *U*(iso) | Atom | *x/a* | *y/b* | *z/c* | *U*(iso) |
| O11 | 0.2793(8) | 0.260(1) | 0.1307(2) | 0.0525 | C32 | −0.217(2) | 0.217(3) | −0.0147(3) | 0.1149 |
| O12 | 0.374(1) | 0.148(1) | 0.3475(2) | 0.0782 | H321 | −0.230(2) | 0.095(3) | −0.0114(3) | 0.1300 |
| O13 | 0.5317(9) | 0.307(2) | 0.3413(2) | 0.0774 | H322 | −0.273(2) | 0.285(3) | −0.0054(3) | 0.1300 |
| C39 | 0.297(1) | 0.249(2) | 0.1585(3) | 0.0450 | C33 | −0.100(1) | 0.258(2) | −0.0008(3) | 0.0888 |
| C42 | 0.345(1) | 0.233(3) | 0.2155(3) | 0.0342 | H331 | −0.084(1) | 0.380(2) | −0.0023(3) | 0.1390 |
| C45 | 0.368(1) | 0.232(2) | 0.2453(2) | 0.0303 | H332 | −0.040(1) | 0.193(2) | −0.0093(3) | 0.1390 |
| C48 | 0.414(1) | 0.229(2) | 0.3026(3) | 0.0378 | C34 | −0.085(1) | 0.224(2) | 0.0291(3) | 0.0802 |
| C51 | 0.436(1) | 0.226(2) | 0.3323(3) | 0.0539 | H341 | −0.102(1) | 0.101(2) | 0.0306(3) | 0.1050 |
| C40 | 0.212(1) | 0.177(2) | 0.1746(2) | 0.0555 | H342 | −0.144(1) | 0.289(2) | 0.0376(3) | 0.1050 |
| H40 | 0.139(1) | 0.128(2) | 0.1667(2) | 0.0690 | C35 | 0.033(1) | 0.261(2) | 0.0439(3) | 0.0794 |
| C41 | 0.239(1) | 0.175(2) | 0.2020(3) | 0.0521 | H351 | 0.052(1) | 0.381(2) | 0.0406(3) | 0.0920 |
| H41 | 0.177(1) | 0.140(2) | 0.2128(3) | 0.0580 | H352 | 0.090(1) | 0.187(2) | 0.0363(3) | 0.0920 |
| C43 | 0.426(1) | 0.296(2) | 0.1979(2) | 0.0488 | C36 | 0.045(1) | 0.225(2) | 0.0737(3) | 0.0698 |
| H43 | 0.497(1) | 0.352(2) | 0.2055(2) | 0.0660 | H361 | 0.024(1) | 0.106(2) | 0.0769(3) | 0.0900 |
| C44 | 0.405(1) | 0.302(2) | 0.1702(3) | 0.0520 | H362 | −0.012(1) | 0.301(2) | 0.0812(3) | 0.0900 |
| H44 | 0.465(1) | 0.338(2) | 0.1588(3) | 0.0600 | C37 | 0.163(1) | 0.260(2) | 0.0885(2) | 0.0711 |
| C46 | 0.293(1) | 0.145(2) | 0.2629(3) | 0.0403 | H372 | 0.182(1) | 0.380(2) | 0.0854(2) | 0.1000 |
| H46 | 0.220(1) | 0.097(2) | 0.2550(3) | 0.0540 | H372 | 0.219(1) | 0.186(2) | 0.0803(2) | 0.1000 |
| C47 | 0.314(1) | 0.143(2) | 0.2901(2) | 0.0381 | C38 | 0.163(1) | 0.226(2) | 0.1183(2) | 0.0625 |
| H47 | 0.263(1) | 0.072(2) | 0.3003(2) | 0.0420 | H381 | 0.104(1) | 0.294(2) | 0.1266(2) | 0.1070 |
| C49 | 0.492(1) | 0.314(2) | 0.2859(3) | 0.0441 | H382 | 0.149(1) | 0.105(2) | 0.1215(2) | 0.1071 |
| H49 | 0.563(1) | 0.372(2) | 0.2932(3) | 0.0590 | C52 | 0.563(2) | 0.324(3) | 0.3710(3) | 0.1083 |
| C50 | 0.467(1) | 0.31202) | 0.2582(3) | 0.0502 | H521 | 0.511(2) | 0.251(3) | 0.3805(3) | 0.1110 |
| H50 | 0.522(1) | 0.367(2) | 0.2470(3) | 0.0480 | H522 | 0.563(2) | 0.439(3) | 0.3787(3) | 0.1110 |
| C31 | −0.232(2) | 0.245(3) | −0.0439(3) | 0.1223 | C53 | 0.672(2) | 0.254(3) | 0.3768(3) | 0.1210 |
| H311 | −0.312(2) | 0.211(3) | −0.0488(3) | 0.1140 | H531 | 0.702(2) | 0.246(3) | 0.3954(3) | 0.1160 |
| H312 | −0.222(2) | 0.366(3) | −0.0480(3) | 0.1140 | H532 | 0.670(2) | 0.140(3) | 0.3689(3) | 0.1160 |
| H313 | −0.179(2) | 0.177(3) | −0.0540(3) | 0.1140 | H533 | 0.723(2) | 0.328(3) | 0.4671(3) | 0.1160 |



Table 2. Some parameters characterizing the conformations of the two molecules of the asymmetric unit of the $Cr_1$ phase of 28OBC.

| | Angle/° | |
|---|---|---|
| Angle between: | Molecule 1 | Molecule 2 |
| Octyloxy chain and adjacent phenyl ring | 11.3 | 7.4 |
| The phenyl rings | 5.8 | 9.3 |
| Ester group and adjacent phenyl ring | 10.0 | 3.0 |
| Torsion angle of the ethyl group | −108.7 | 122.7 |

parallel to the long axes of the molecules. Since the layer spacings of both phases are equal (table 3), for TFS films of 28OBC the condition of zero tilt is not only fulfilled in the E phase, but also in the crystalline $Cr_{4C}$ phase.

In many crystalline phases of liquid crystalline compounds the molecular long axes are oriented more or less parallel to the *c*-direction of the respective unit cells [20–22]. This is also the case in the $Cr_1$ phase. Therefore we assume the zone axis for the investigations of the TFS films with parallel beam geometry to be approximately the [0 0 1]-axis. In this case the observed in-plane structure of the smectic layers can be assigned to the (*h k* 0) plane. A complete structural determination of the $Cr_{4C}$ phase was not possible by this method since the diffractograms obtained from oblique beam incidence could not be indexed.

The TFS films investigated by electron diffraction had been transferred without annealing of the original FS films. Therefore they are composed of different islands with lateral dimensions up to 0.1 mm and with different thicknesses. From the different interference colours, the thicknesses of the thinnest islands investigated were determined to be 200 Å. In this thickness range the

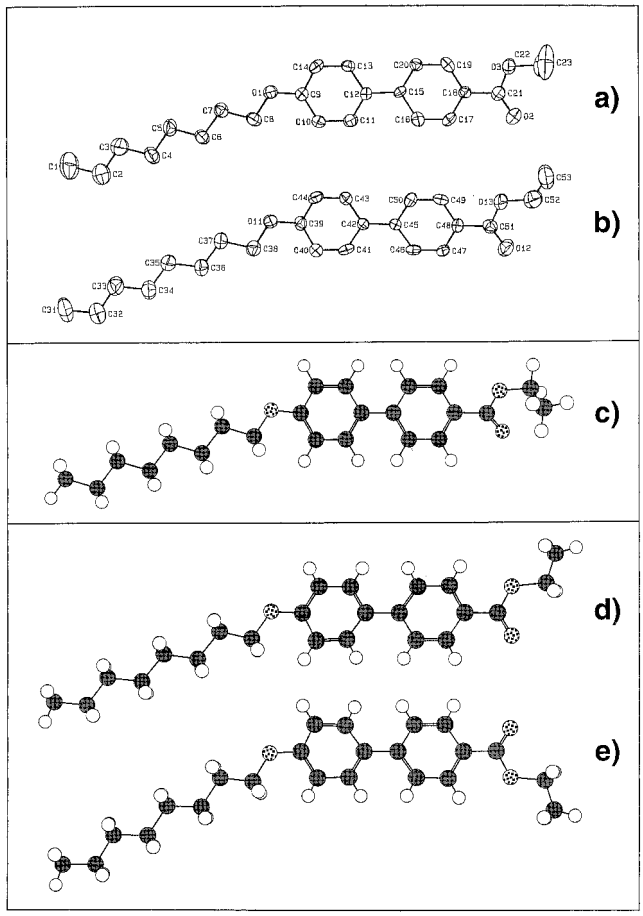


Figure 3. Molecular structures of 28OBC in the projections to the plane of the phenyl rings: (*a*) and (*b*) ORTEP plots of the two independent molecules of the asymmetric unit of the $Cr_1$ phase showing the atomic labelling scale; (*c*) molecular structure after optimizing the two molecules (*a* and *b*) by semi-empirical MO calculations; (*d*) *trans*- and (*e*) *cis*-like planarized molecules derived from molecule 1 and used for the simulation of electron diffractograms.

accuracy of this method is $\pm 1$ layer (corresponding to $\pm 25$ Å). By cooling the films to ambient temperature (into the $Cr_{4C}$ phase) each island splits into many crystalline domains. Due to the average area of these domains being in the μm-range [14] and within the diameter of the electron beam, often more than one domain is irradiated simultaneously. The corresponding diffraction picture therefore results from all simultaneously measured domains and shows several similar diffraction patterns rotated against each other. The rotation angle between two respective patterns corresponds to the different directions of the two-dimensional crystallographic axes in the two domains. The observed angles were different in all cases. A relation between them was not found.

From domains with lateral dimensions larger than the electron beam, single crystal electron diffractograms of TFS films of 28OBC in the $Cr_{4C}$ phase at ambient temperature have been obtained. Independent of the respective domain thickness, all these diffractograms showed the same pattern. A typical example is shown in figure 6 (*a*). The large number of sharp ($h\,k\,0$) reflections corresponds to a crystalline two-dimensional lattice. The equal intensity of each set of four reflections ($h\,k\,0$) with $h = \pm h$, $k = \pm k$ further indicates that it is of a rectangular type and excludes triclinic plane groups. The lattice parameters are $a = 5.6 \pm 0.1$ Å, $b = 7.8 \pm 0.2$ Å and $\gamma = 90°$ as given in table 3.

These parameters show remarkable similarities to the corresponding parameters of the $Cr_1$ phase. The $b$ and $\gamma$ values of both phases are equal within experimental error and the $a$ value of $Cr_1$ is exactly twice as large as the corresponding value for $Cr_{4C}$. This allows us to assume that the $Cr_{4C}$ phase is a crystalline high temperature phase compared to $Cr_1$, gaining symmetry by reducing the number of molecules per unit cell and also supports the assumption of the [0 0 1] zone axis made above. The ratio of the $a$ values of $Cr_{4C}$ and $Cr_1$ suggests a unit cell in the films with half ($Z = 4$) or a quarter ($Z = 2$) of the cell volume of the bulk phase. This argument will be important for the reduction of reasonable space groups for the $Cr_{4C}$ phase (see § 3.2.3).

Interestingly, the intensities of the ($0\,k\,0$) reflections with $k = 2n + 1$ are comparatively weak. This can be interpreted in two ways. Firstly, these reflections are considered as 'real' but weak. In this case no extinctions can be observed, which reduces the possible two-dimensional plane groups of the density projection on the [0 0 1] zone to *pm* and *pmm*. However, the weakness of these reflections suggests that here the deviation from a more symmetric structure, exhibiting a $2_1$-screw axis or glide plane, is only gradual. The second possibility results from the thickness of the films. Since all TFS films were thicker than ≈200 Å, weak diffraction spots may arise at positions of systematic absences due to dynamical scattering [23]. Assuming the absences of the ($0\,k\,0$) reflections with $k = 2n + 1$ in figure 6 (*a*), the possible plane groups of the density projection to the [0 0 1] zone are *pg* and *pmg*.

The plane groups *pmm* and *pmg* require four molecules at general positions. To build up a unit cell containing two molecules, the molecules must be positioned at special equivalent positions of the unit cell and the molecule itself must exhibit a mirror plane. Although a mirror plane in the molecular geometry of 28OBC is a special case (and for instance not observed in the single crystal structure), it is possible and therefore the plane groups *pmm* and *pmg* need to be considered for the

derivation of symmetry-allowed space groups from the projection to their *ab* plane (§ 3.2.3).

3.2.2. *Electron diffraction on the E phase*

When heating the TFS films to temperatures above 73°C, a diffraction pattern similar to the pattern already observed from FS films in an E phase [10] appears (figure 4). In this pattern only some of the low order reflections, i.e. the (1 1 0), (1 2 0), (1 3 0) and (0 2 0) reflections, remain visible. The loss of the higher order reflections is due to a larger molecular mobility in the less ordered E phase compared with the crystalline phase. This increase in molecular mobility has two more consequences. Firstly, it leads to an increase of the symmetry of the density projection, visible by the absence of the (1 0 0) and (0 1 0) reflections in the pattern. Secondly, it leads to an increase of the two-dimensional unit cell area. The unit cell dimensions of the E phase are $a = 5.6 \pm 0.1$ Å, $b = 8.2 \pm 0.1$ Å and $\gamma = 90°$ (table 3). Therefore the increase of the unit cell area interestingly results from an increase of one lattice parameter only. The change of the unit cell volume by cooling TFS films from the E phase to the crystalline phase has already been observed macroscopically by the development of cracks [13, 14].

3.2.3. *Simulation of electron diffraction pattern*

The simulation of transmission electron diffraction patterns has been used for two purposes. Firstly, using data from the experimental diffractograms combined with molecular geometries, SAXR results and packing energies, a structural model for the $Cr_{4C}$ phase is proposed. Secondly, the calculated pattern of the single crystalline $Cr_1$ phase, known from X-ray analysis, is compared with experimental diffractograms of the $Cr_{4C}$ film phase.

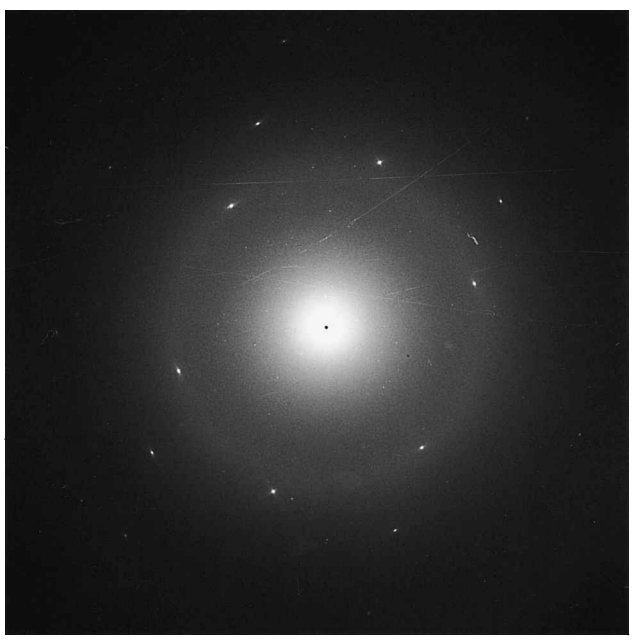

Figure 4. Typical diffraction pattern of TFS films of 28OBC in the E phase at 73°C. The halo arises from the carbon substrate.

As already mentioned, a complete structure determination of the $Cr_{4C}$ phase could not be carried out because information from other zone axes could not be obtained. In order to propose a structure for this phase from simulations of electron diffraction patterns, the number of potential space groups has to be reduced.

Following the argument about cell volume given in § 3.2.1 [$a$(TED) = 0.5*$a$(SCXRD)] and considering the observation of all (0 0 $l$) reflections up to $l = 6$ in SAXR diffractograms (see § 3.3) of the $Cr_{4C}$ phase [$c$(SAXR) = 0.5*$c$(SCXRD)], only space groups containing two molecules are possible. Therefore only the five monoclinic groups $P2$ (*pm* projection), $P2_1$ (*pg* projection), $Pm$ (*pm* projection), $P2/m$ (*pmm* projection) and $P2_1/m$ (*pmg* projection) and the two orthorhombic groups $Pmm2$ (*pmm* projection) and $Pma2$ (*pmg* projection) remain.

The geometry of the single molecules in the $C_{4C}$ phase and therefore the asymmetric unit for the simulations is also unknown. As expected from packing considerations, non-planar molecular geometries were planarized when either the single crystal or the MOPAC geometry was packed in unit cells with desired dimensions. For this reason and in order to consider the special case of asymmetric units containing a mirror plane, planarized geometries with *cis*-like and *trans*-like orientations of the ethyl group with respect to the octyloxy chain were derived from molecule 1 of the $Cr_1$ crystal structure, figures 3 (*d*) and 3 (*e*). The *cis*-like form was still quite difficult to pack into the unit cells and therefore only the *trans*-like form was used for extensive simulations of electron diffraction patterns.

In the case of the space groups $P2_1/m$, $Pma2$, $P2/m$ and $Pmm2$, the two molecules of the unit cell need to be positioned at a mirror plane. In the latter two cases (*pmm* projections) the molecules must be packed in rows which is not possible in unit cells with the experimental $a$ and $b$ values. The overlap of molecules by this kind of packing is exemplarily shown in the case of a $Pmm2$ unit cell in figure 5 (top). Therefore these two space groups can be excluded. The packing of two molecules at special equivalent positions for the space groups $P2_1/m$ and $Pma2$ with acceptable minimum packing energies is possible (figure 5, bottom), but in these cases the simulated electron patterns are clearly different from the measured diffractogram. However, the restriction of symmetry-allowed molecular translations to two and of molecular rotations to one direction, does not

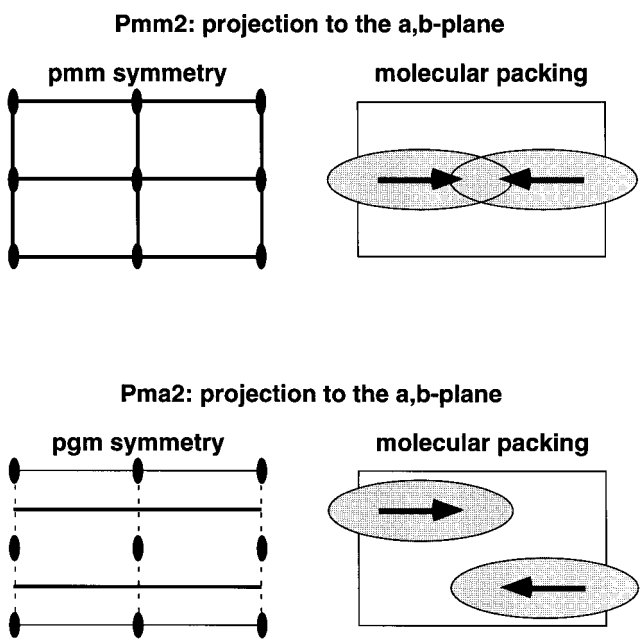


Figure 5. Symmetry considerations by packing two 28OBC molecules containing mirror planes in unit cells of space groups with *pmm* or *pmg* symmetry in their respective rectangular projection to the *ab*-plane. Displayed are the projections of the symmetry elements (left hand side) and schematically one respective possibility of molecular packing (right hand side) for the representative examples of the *Pmm*2 (top) and *Pma*2 (bottom) space groups. The light grey ovals in the packing drawings (right hand side) represent the projection of the single molecules on to the *ab*-plane with a mirror plane parallel to their length axes. The arrows inside these ovals indicate the absence of a second mirror plane perpendicular to the first. The dimensions of the molecule and unit cell projections are arbitrary and do not correspond to experimental data. In both cases (*pmm* and *pmg* projection), the molecular mirror planes must coincide with the unit cell mirror planes, which strongly reduces the number of allowed molecular orientations in the cells.



allow refinement of the simulated diffraction pattern and therefore these two space groups can also be excluded.

Unit cells of the remaining three monoclinic space groups $P2$, $Pm$ and $P2_1$ can be built up containing two molecules at general equivalent positions. These molecules do not need mirror planes or other symmetry elements (except of the identity) and in contrast to the four space groups discussed above their orientations within the unit cells are not limited by symmetry arguments (except of the orientation in relation to each other). As a result using the $P2$, $Pm$ and $P2_1$ space group, unit cells with different molecular orientations and satisfying packing energies could be simulated, respectively, according to the procedure described in § 2.

The simulation of electron diffraction patterns for the three remaining cells, as also described in the experimental section, was used to judge the various structural suggestions. In the case of the space groups $Pm$ and $P2$ no simulated patterns similar to the experimental patterns could be obtained. Indeed these patterns displayed weak $(0\ k\ 0)$ reflections with $k = 2n + 1$, but the intensity ratios of the other reflections were clearly wrong in comparison with the experimental diffraction pattern. The simulations with $P2_1$ structures resulted in the closest simulated patterns as compared with the measured diffractogram, but exhibit systematic absences at the positions mentioned above. One of the best calculated patterns is shown in figure 6(*b*). This pattern directly corresponds to a structure with minimum packing energy ($-51$ kcal mol$^{-1}$). Its unit cell has a $c$ axis of $c = 24.6$ Å, a monoclinic angle $\beta = 94.0°$ and a desnity $d_x = 1.10$ g cm$^{-3}$, figures 6(*c*) and 6(*d*). In this structure the molecules are oriented in layers and the octyloxy chains of neighbouring molecules point in opposite directions, similar to the $Cr_1$ phase. Both pattern and packing energy deteriorate significantly by changing the orientation of the molecules more than 2° with respect to the $x$- or $y$-axes and more than 5° with respect to the $z$-axis of the unit cell.

In order to compare the structure obtained for the $Cr_{4C}$ phase with the structure of the $Cr_1$ crystal phase, the diffraction pattern of the latter phase along the [0 0 1] zone axis was calculated from the single crystal X-ray data (the crystals of the $Cr_1$ phase were too thick for transmission electron diffraction). In this pattern, figure 6(*e*), the reflections along the $a^*$-direction have exactly half the periodicity of the corresponding set of reflections in the diffractogram of the $Cr_{4C}$ phase, figure 6(*a*). This shows again the doubling of the lattice parameter as already mentioned in § 3.2.1. In order to generate the $Cr_{4C}$ diffraction pattern based on the $Cr_1$ structure, one of the symmetrically independent molecules was cancelled and the $a$-axis was divided by two. By this method again, a $P2_1/c$ unit cell results. Due to the glide plane of this symmetry, the resulting simulated diffraction pattern, figure 6(*f*), also has the extinctions shown in figure 6(*b*). However, the space group $P2_1/c$ of the $Cr_1$ phase contains the simulated space group $P2_1$ of the $Cr_{4C}$ phase as a sub-group. Therefore it was possible to generate a $P2_1$ unit cell from the $Cr_1$ phase. The resulting structure and its corresponding simulated electron diffraction pattern are given in figures 6(*g*) and 6(*h*), respectively.

The comparison of the structure obtained from pure simulation with the structure obtained from reducing the symmetry of the SCXRD structure gives only small differences. In the case of the simulated structure the conformation of the molecule was fixed to be planar, which leads to slightly different orientations of the molecules

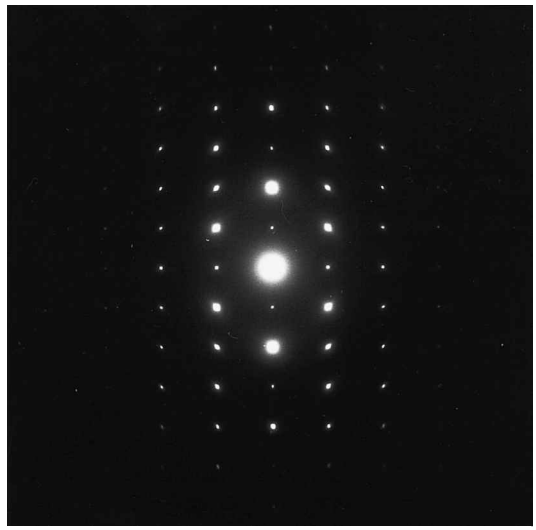

(*a*)

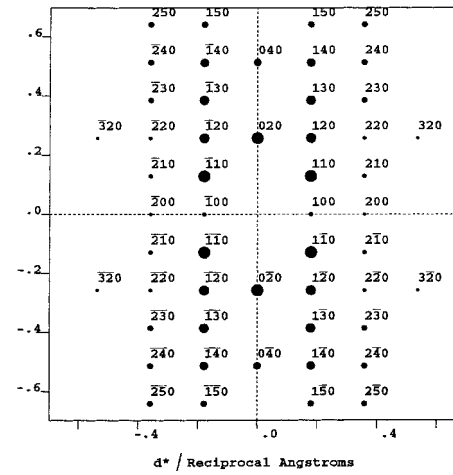


(*b*)



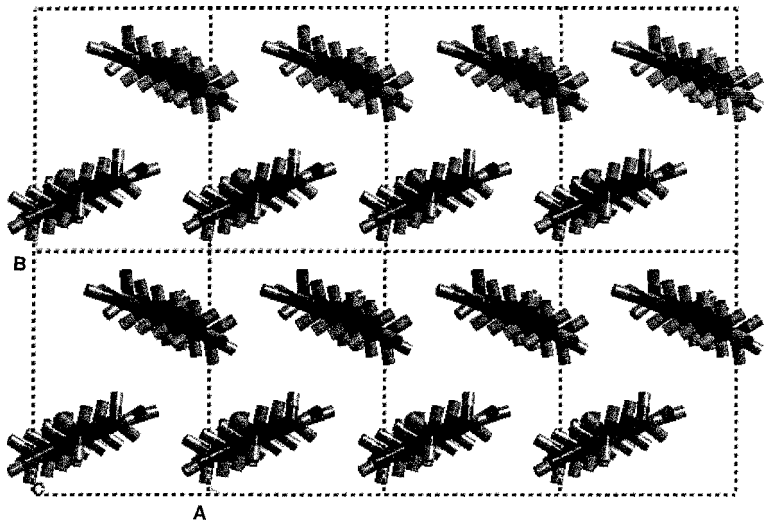


(*c*)

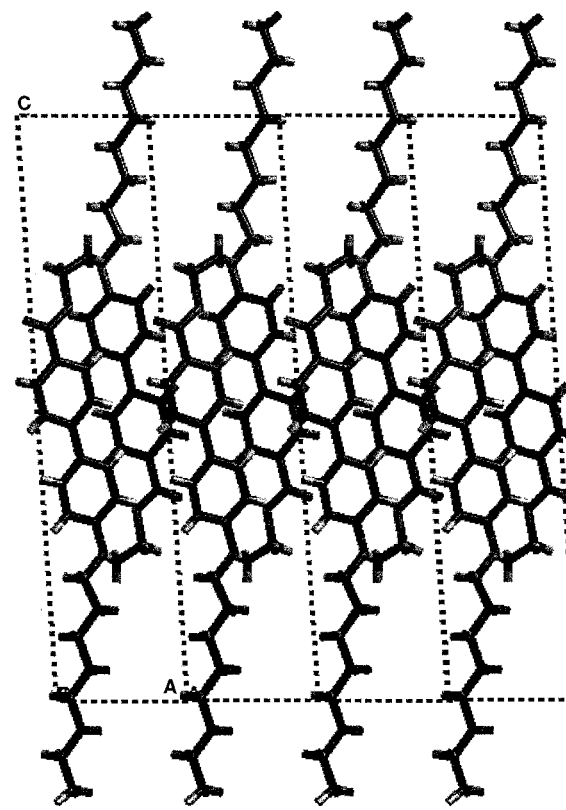


(*d*)

Figure 6. Measured and simulated transmission electron diffraction patterns of TFS films of 28OBC. All patterns correspond to the [0 0 1] zone axis with the $b$*-axis oriented vertically and the $a$*-axis oriented horizontally. (*a*) Typical measured diffraction pattern of the crystalline $Cr_{4C}$ phase at ambient temperature; (*b*) simulated pattern of the calculated $P2_1$ structure; (*c*) view of the $P2_1$ structure along the $c$-axis ($2 \times 3$ unit cells) and (*d*) along the $b$-axis (4 unit cells); (*e*) calculated pattern of the $Cr_1$ phase; (*f*) calculated pattern of $P2_1/c$ structure obtained from the $Cr_1$ phase; (*g*) calculated pattern of a monoclinic $P2_1$ structure obtained from the $Cr_1$ phase; (*h*) $2 \times 3$ unit cells of the $Cr_1$ phase after symmetry reduction from $P2_1/c$ ($Z = 8$) to $P2_1$ ($Z = 2$).

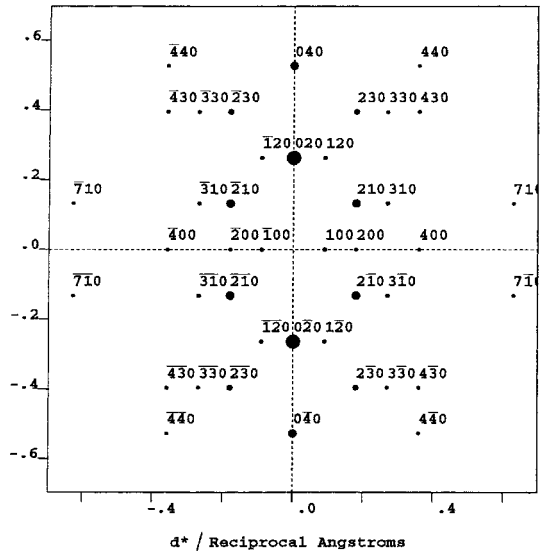


(*e*)

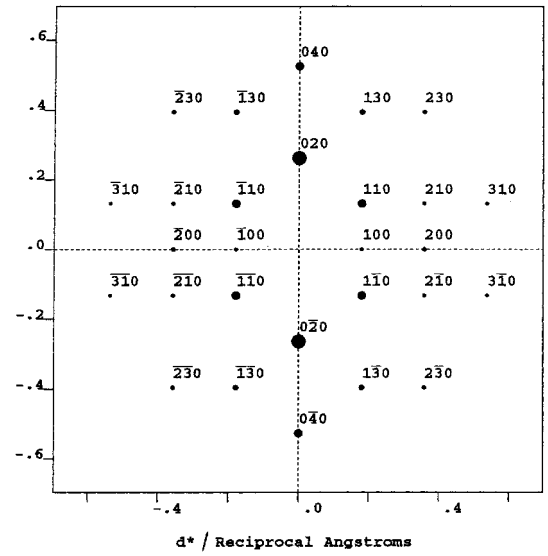


(*f*)



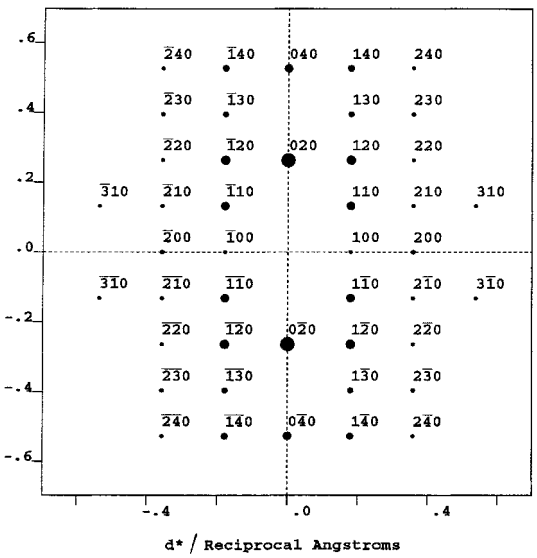


(*g*)

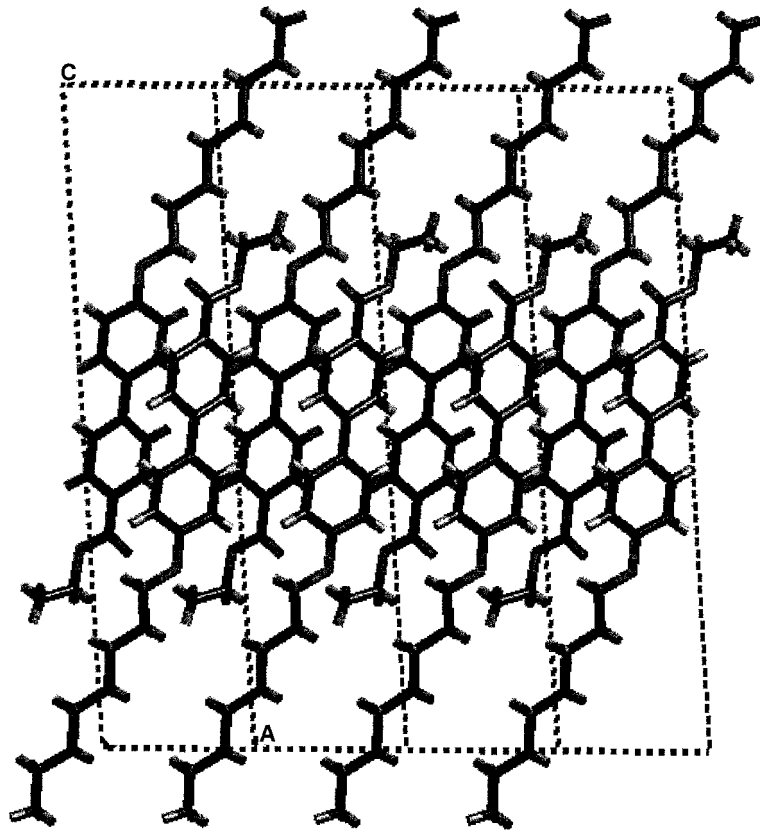


(*h*)

Figure 6. (*continued*).

in the cell. However, a screwed molecule can be packed better and therefore the structure obtained from SCXRD exhibits a better packing energy of $-73$ kcal mol$^{-1}$. The diffraction patterns of both structures are comparable, although the differences in orientation and conformation of the molecules cause slight shifts of the intensities.

### 3.3. *Structural comparison of the phases in thin films and bulk*

In this and previous papers [13, 15] we have investigated the structures of different phases of 28OBC in bulk, Langmuir–Blodgett and transferred freely-suspended films. In order to discuss the structural relationships between these phases, parameters of the respective elementary cells are listed in table 3.

Even in bulk, 28OBC exhibits more than one crystalline phase ($Cr_1$, $Cr_2$ and $Cr_3$). These phases cannot be distinguished by X-ray powder diffraction. Particularly, their 'smectic' layer spacings are identical in all cases ($d = 24.6 \pm 0.2$ Å). Therefore it is concluded that the unit cell dimensions of the phases must be similar and the structures probably differ slightly in their molecular conformations. Another hint as to the similarity of $Cr_1$ and $Cr_3$ is their common transition temperature to the LC phases. Presently, more conclusions about the relationship of the bulk phases are not possible.

In the discussion of the structure of the $Cr_1$ phase, we have already pointed out that the dipole moments of neighbouring molecules in the layers point in opposite directions. This leads to an understanding of our recently observed rearrangement process taking place in Langmuir–Blodgett films of 28OBC [15]. By the deposition conditions of the Langmuir–Blodgett method, the formation of a bilayer structure (assigned as $Cr_5$, figure 1) with a layer spacing of 43.7 Å (table 3) is enforced. This structure rearranges at ambient temperature within hours into a monolayer structure (assigned as $Cr_6$, figure 1) with a layer spacing of 24.2 Å (table 3). Even though many different forces are responsible for structure formation, one of the driving forces of this rearrangement process may be the change of the enforced parallel arrangement into the more favourable, bulk-like dipole arrangement of neighbouring molecules.

Comparison of the 'smectic' layer spacings $d_{00l}$ shows that, dependent on the respective substrate, in TFS films of 28OBC crystalline phases with different structures exist (table 3, figure 1). Obviously these phases differ not only in their layer spacings, but also in their in-plane structures (table 3). However, it has to be mentioned that the $a$, $b$ and $\gamma$ values of the $Cr_{4O}$ phase were obtained by AFM measurements and therefore arise from the surface layer of the film [14]. These values are not necessarily also valid for the inner film structure and also may not correspond to the given $c$ value. Nevertheless, from the layer spacing alone, it is obvious that the structure of $Cr_{4O}$ must be different from that of the crystalline bulk phases. In the case of the $Cr_{4C}$ phase, the layer spacing is identical to that of the crystalline bulk phases ($d = 24.5 \pm 0.2$ Å), but the difference between the $Cr_{4C}$ and the $Cr_1$ phases has been shown by the simulation of the electron diffraction pattern of the latter. An influence of the substrate on the structure of ultra-thin organic films has also been reported for Langmuir–Blodgett monolayers on different solid supports [24, 25].

## 4. Summary and conclusion

The crystal and molecular structure of one of the crystalline phases (assigned as $Cr_1$) of ethyl 4′-*n*-octyloxybiphenyl-4-carboxylate (28OBC) was determined by single crystal X-ray diffraction. In this structure the molecules are oriented in layers parallel to the (0 0 1) plane, similar to a known structure of another 4′-substituted biphenyl-

Table 3. Structural data of different phases of 28OBC as obtained by single crystal X-ray diffraction (SCXRD), small angle X-ray reflection (SAXR), transmission electron diffraction (TED) and atomic force microscopy (AFM). Substrates: C = carbon coated substrate; Q/O = quartz coated with octadecyltrichlorosilane (OTS); Si/O = silicon coated with octadecyltrichlorosilane (OTS).

| | | | in-plane structure | | | | | |
|---|---|---|---|---|---|---|---|---|
| Phase | $T$/°C | Substrate | Method | $a$/Å | $b$/Å | $\gamma$/° | $A$[a]/Å$^2$ | $d_{00l}$[b]/Å |
| $Cr_1$ | 25 | — | SCXRD | 11.2 | 7.6 | 90 | 21.3 | 24.5[c] ± 0.2 |
| $Cr_2$ | 25 | — | —[d] | —[d] | —[d] | —[d] | —[d] | 24.5 ± 0.2 |
| $Cr_3$ | 25 | — | —[d] | —[d] | —[d] | —[d] | —[d] | 24.5 ± 0.2 |
| $Cr_{4O}$ | 25 | Q/O | AFM | 5.8 ± 0.3 | 7.3 ± 0.4 | 71 | 19.0 | 23.6 ± 0.2 |
| $Cr_{4C}$ | 25 | C | TED | 5.6 ± 0.1 | 7.8 ± 0.2 | 90 | 21.8 | 24.5 ± 0.2 |
| $Cr_5$ | 25 | Si/O | —[d] | —[d] | —[d] | —[d] | —[d] | 43.7 ± 0.2 |
| $Cr_6$ | 25 | Si/O | —[d] | —[d] | —[d] | —[d] | —[d] | 24.2 ± 0.2 |
| E | 91 | C | TED | 5.6 ± 0.1 | 8.2 ± 0.1 | 90 | 23.0 | 24.5 ± 0.2 |

[a] Area $A$ per molecule of the projection on the $ab$-plane.
[b] All layer spacings $d_{00l}$ were obtained by SAXR.
[c] In the case of the $Cr_1$ phase the observed $d_{00l}$ spacing is only half of the actual $c$ lattice parameter of the unit cell ($c = 49.1$ Å) caused by the $P2_1/c$ symmetry.
[d] Not investigated.

4-carboxylate [20]. Interestingly, the structures of thin crystalline TFS films depend on the substrate ($Cr_{4C}$ and $Cr_{4O}$ phases) and also differ from the structure of the $Cr_1$ bulk phase. We conclude, that the film phases are metastable high temperature phases in which the elementary cells contain fewer molecules than the cell of the low temperature $Cr_1$ phase. This can be explained by an increased mobility of molecules and molecule segments at higher temperatures, leading to more equivalent molecule positions. From packing and symmetry arguments and simulations of electron diffraction patterns, we are able to suggest a monoclinic unit cell of the $P2_1$ space group as a possible structure of the $Cr_{4C}$ phase. Interestingly, this is also the space group of the other biphenyl-4-carboxylate mentioned above. The simulated structure turns out to be close to the structure which results from cancelling one of the symmetrically independent molecules and additional symmetry reduction from $P2_1/c$ to $P2_1$ of the SCXRD structure of $Cr_1$. Another example of such a behaviour is the crystalline phases of biphenyl, where in a low temperature phase one lattice parameter is twice that in the room temperature phase [26, 27]. The assumption that the film phases of TFS films are high temperature phases is reasonable since they form by cooling from the E phase and therefore will be influenced by its structure. The result of this influence is a similar structure in both phases—compare the diffraction patterns, figures 4 and 6(*a*), and the lattice parameters. It should be emphasized that the only way to make thin films with the structural characteristics discussed above is by employing the liquid crystalline properties of 28OBC, namely the capability of 28OBC to form freely-suspended liquid crystalline films and to transfer these films onto solid supports.

The creation of new thin film structures by cooling TFS films from their LC phases should also be possible with other liquid crystalline materials and might be relevant for various purposes. With respect to our results on E/crystalline transitions, it should be interesting also to study cases of thin films which possess phase transitions from hexatic phases (SmB, SmF, SmI) or even less ordered smectic phases (SmA, SmC) directly to a crystalline phase.

We are grateful to H. Möhwald and I. Voigt-Martin for access to the electron microscope and to the molecular simulation hard- and soft-ware. We also wish to thank them for helpful discussions. This work was further supported by the Bundesministerium für Bildung, Wissenschaft, Forschung und Technologie (BMBF) and by the Deutsche Forschungsgemeinschaft (DFG).



## References

[1] Young, Ch. Y., Pindak, R., Clark, N. A., and Meyer, R. B., 1978, *Phys. Rev. Lett.*, **40,** 773.
[2] Pindak, R., and Moncton, D., 1982, *Physics Today*, **35,** 57.
[3] Decher, G., Reibel, J., Honig, M., Voigt-Martin, I. G., Dittrich, A., Ringsdorf, H., Poths, H., and Zentel, R., 1993, *Ber. Bunsenges. phys. Chem.*, **97,** 1386.
[4] Reibel, J., Brehmer, M., Zentel, R., and Decher, G., 1995, *Adv. Mater.*, **10,** 852.
[5] Gierlotka, S., Lambooy, P., and de Jeu, W., 1990, *Europhys. Lett.*, **12,** 341.
[6] Tweet, D. J., Holyst, R., Swanson, B. D., Stragier, H., and Sorensen, L. B., 1990, *Phys. Rev. Lett.*, **65,** 2157.
[7] Lambooy, P., Gierlotka, S., Hamley, I. W., and de Jeu, W., 1992, in *Phase Transitions in Liquid Crystals*, edited by S. Martellucci, and A. N. Chester (New York: Plenum Press).
[8] Sirota, E. B., Pershan, P. S., Sorensen, L. B., and Collett, J., 1987, *Phys. Rev. A*, **36,** 2890.
[9] Cheng, M., Ho, J. T., Hui, S. W., and Pindak, R., 1987, *Phys. Rev. Lett.*, **59,** 1112.
[10] Cheng, M., Ho, J. T., Hui, S. W., Goodby, J. W., Pindak, R., Geer, R., and Huang, C. C., 1991, *Phys. Rev. A, Rapid Commun.*, **44,** R7891.
[11] Maclennan, J., Decher, G., and Sohling, U., 1991, *Appl. Phys. Lett.*, **59,** 917.
[12] Decher, G., Maclennan, J., Reibel, J., and Sohling, U., 1991, *Adv. Mater.*, **3,** 617.
[13] Decher, G., Maclennan, J., Sohling, U., and Reibel, J., 1992, *Thin Solid Films*, **210/211,** 504.
[14] Overney, R. M., Meyer, E., Frommer, J., Güntherodt, H.-J., Decher, G., Reibel, J., and Sohling, U., 1993, *Langmuir*, **9,** 341.
[15] Decher, G., and Sohling, U., 1991, *Ber. Bunsenges. phys. Chem.*, **95,** 1538.
[16] Decher, G., Maclennan, J., and Reibel, J., 1991, *Ber. Bunsenges. phys. Chem.*, **95,** 1520.
[17] Stewart, J. P., *MOPAC 6.0*, QCPE No. 455, Creative Arts Building 181, Indiana University, Bloomington, IN 47405, USA.
[18] Stapleton, M., *Cerius V3.2*, Molecular Simulations INC., 16 New England Executive Park, Burlington, MA 01803-5297, USA.
[19] Gray, G. W., and Goodby, J. W., 1976, *Mol. Cryst. liq. Cryst.*, **37,** 157.
[20] Hori, K., Takamatsu, M., and Ohashi, Y., 1989, *Bull. chem. Soc. Jpn.*, **62,** 1751.
[21] Vani, G. V., 1983, *Mol. Cryst. liq. Cryst.*, **99,** 21.
[22] Hori, K., and Ohashi, Y., 1991, *Liq. Cryst.*, **9,** 383.
[23] Cowley, J. M., 1986, *Diffraction Physics*, 2nd Edn (Amsterdam-New York: North-Holland Personal Library).
[24] Engel, M., Merle, H. J., Peterson, I. R., and Steitz, R., 1991, *Ber. Bunsenges. phys. Chem.*, **95,** 1514.
[25] Zasadzinski, J. A., Viswanathan, R., Madsen, L., Garnaes, J., and Schwartz, D. K., 1994, *Science*, **263,** 1726.
[26] Charbonneau, G. P., and Delugeard, Y., 1976, *Acta Cryst.*, **B32,** 1420.
[27] Charbonneau, G. P., and Delugeard, Y., 1976, *Acta Cryst.*, **B33,** 1586.